Journal: ACS Sustainable Chemistry & Engineering

Manuscript ID: sc-2019-016963.R1

Supporting Information

Number of pages: 12 (page S1- page S12)

Number of figures: 8 (Figure S1-Figure S8)

Number of table: 1 (Table S1)

NiS-MoS_2 hetero-nanosheet arrays on carbon cloth for high-performance flexible hybrid energy storage devices

Shundong Guan,[†,‡] Xiuli Fu, [,†] Zhezhu Lao,[§] Chuanhong Jin,[§] and Zhijian Peng[*,‡]*

[†] State Key Laboratory of Information Photonics and Optical Communications, and School of Science, Beijing University of Posts and Telecommunications, Beijing 100876, P. R. China

[‡] School of Science, China University of Geosciences, Beijing 100083, P. R. China

[§] State Key Laboratory of Silicon Materials, School of Materials Science and Engineering, Zhejiang University, Hangzhou, Zhejiang 310027, P.R. China

**Corresponding author*: Prof. Xiuli Fu, Prof. Zhijian Peng

*Email: xiulifu@bupt.edu.cn (X. Fu); pengzhijian@cugb.edu.cn (Z. Peng)

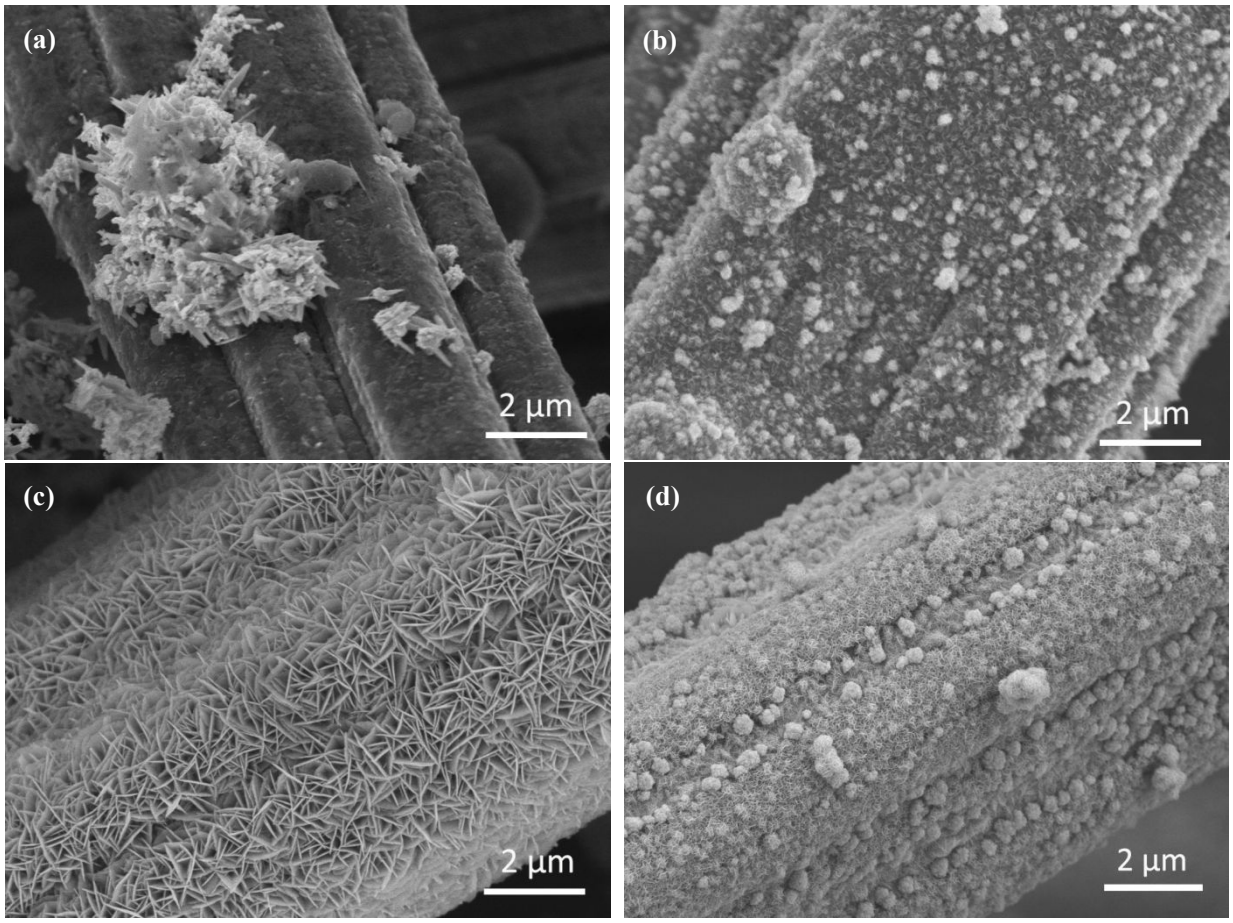

Figure S1. SEM images of NiS-MoS_2 nanostructures on carbon cloth synthesized with different concentrations of sodium dodecyl sulfate (SDS): (a) 0, (b) 0.1, (c) 0.2, and (d) 0.3 mol·L^{-1}.

As shown in **Figure S1**, the concentration of SDS has significant influence on the morphology of the products. Without SDS in the solution, some irregular-shaped nanostructures were formed randomly on the surface of CC (**Figure S1a**), indicating that NiS and MoS_2 couldn't uniformly grow on the surface of CC due to the poor wettability of carbon in aqueous solution. Similarly, when a relatively low concentration (0.1 mol·L^{-1}) of SDS was used, only some small particle or flower-like nanostructures were formed, decorating on the CC (**Figure S1b**). However, when 0.2 mol·L^{-1} SDS was applied, many large nanosheets were uniformly and vertically aligned as nanowalls on the CC (**Figure S1c**). By further increasing the concentration of SDS to 0.3 mol·L^{-1}, the formed nanosheets were aggregated together with a smaller size (**Figure S1d**). Thus, 0.2 mol·L^{-1} of SDS was optimized for the synthesis of NiS-MoS_2 HNSAs.

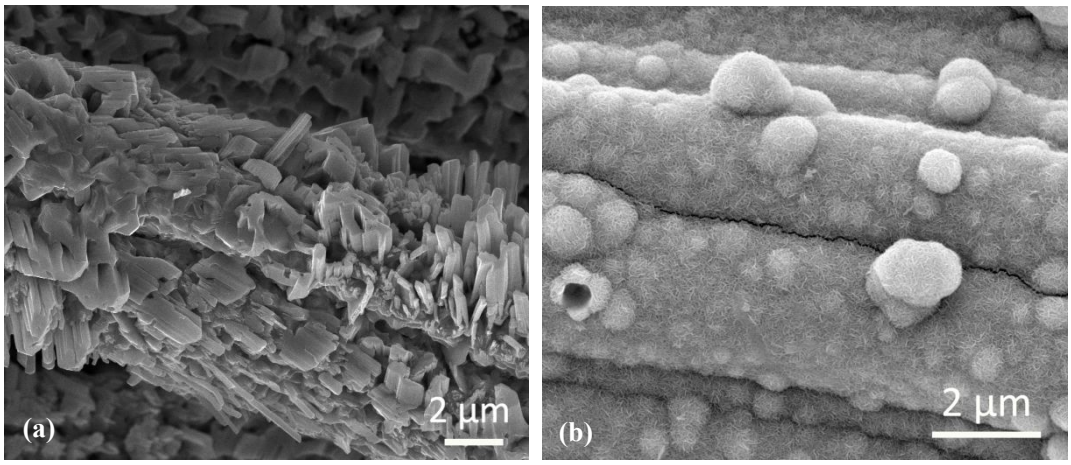

Figure S2. SEM images of pure NiS (a) and MoS_2 (b) nanostructures on CC.

As comparative samples for the NiS-MoS_2 HNSAs/CC, pure NiS and MoS_2 nanostructures were also grown on CC *via* a similar process, respectively. For the NiS/CC, many irregular big nanoparticles are aggregating together and wrapping the CC. For the MoS_2/CC sample, a layer of tiny nanosheets is uniformly coating the CC.

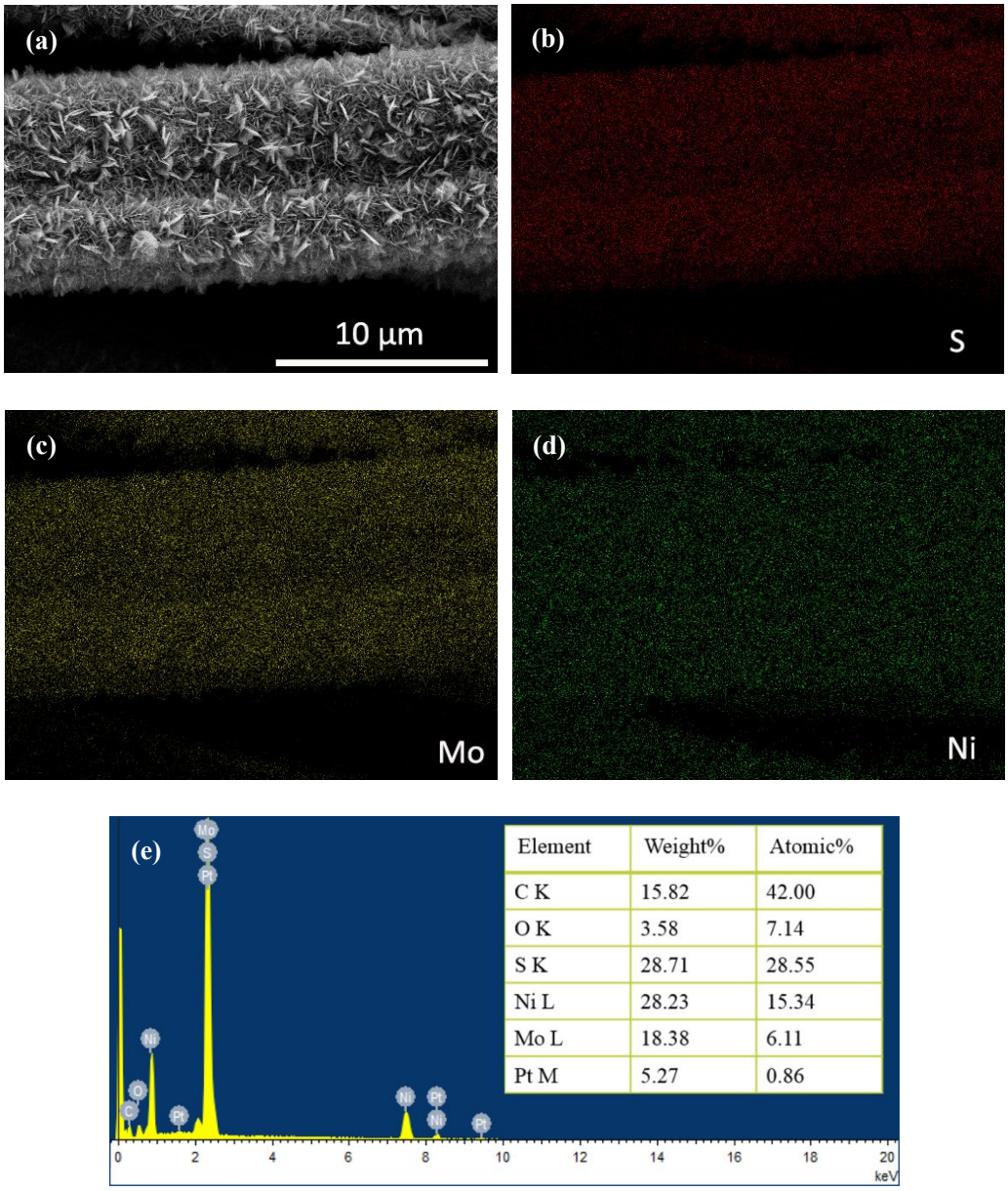

Element	Weight%	Atomic%
C K	15.82	42.00
O K	3.58	7.14
S K	28.71	28.55
Ni L	28.23	15.34
Mo L	18.38	6.11
Pt M	5.27	0.86

Figure S3. SEM-EDX results of NiS-MoS_2 HNSAs/CC. (a) Typical SEM image and the corresponding EDX mapping spectra of S (b), Mo (c) and Ni (d) elements. (e) EDX spectrum, in which the inset shows the table of element contents.

From **Figure S3**, it can be seen that S, Mo and Ni elements are all existing over the whole surface of carbon fiber, indicating that NiS and MoS_2 are uniformly distributing on the carbon cloth (CC). The calculated percentage of MoS_2 in the sample was about 28.5 mol.%. It should be noted that, Pt atoms originate from the sprayed Pt film for the preparation of SEM sample; and O atoms might be derived from the adsorbed O_2 or H_2O on the sample.

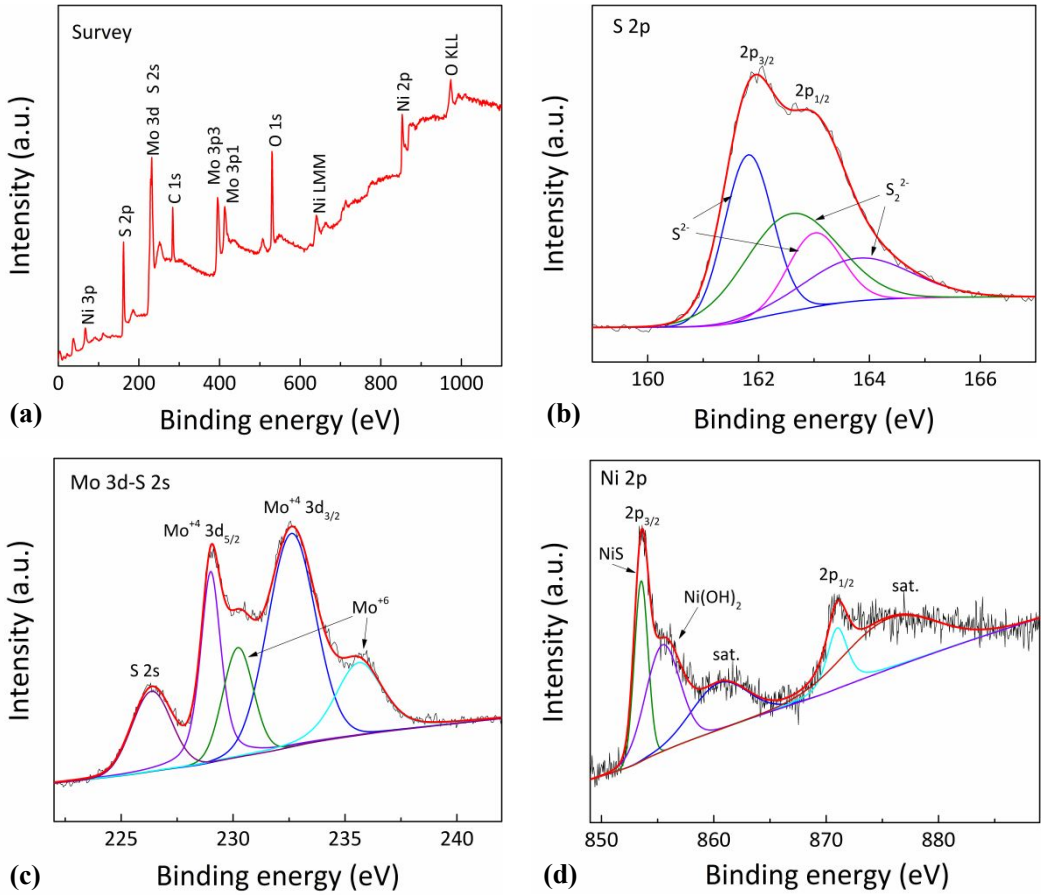

Figure S4. XPS results of NiS-MoS_2 HNSAs/CC. (a) XPS survey spectrum, and high-resolution spectra of S 2p (b), Mo 3d-S 2s (c), and Ni 2p (d).

Figure S4 shows the XPS results of the obtained NiS-MoS_2 HNSAs/CC. The XPS survey spectrum (**Figure S4a**) reveals the existence of S, Mo, Ni, O and C atoms in this sample. In the S 2p high-resolution spectrum (**Figure S4b**), the two main peaks at 161.8 and 162.6 eV can be assigned to those of $2p_{3/2}$ and $2p_{1/2}$ in S^{2-}.[S1] Meanwhile, the coincident binding energies of 162.5 and 163.9 eV could be attributed to those of S_2^{2-}, implying the existence of unsaturated S atoms on Ni-S and/or Mo-S sites, which are correlated with the well-remained electrochemically active sites.[S2] The peak located at 226.3 eV in the Mo 3d-S 2s high-resolution spectrum (**Figure S4c**) can be indexed to S 2s;[S3] the two main peaks at 229.0 and 232.6 eV can be assigned to the $3d_{5/2}$ and $3d_{3/2}$ orbitals of Mo (IV), respectively; and the peaks at 230.2 and 235.6 eV are in accordance with those of Mo (VI) due to its partial oxidation during exposure to air.[S4] In addition, the narrow peaks at 853.5 and 871 eV in the Ni 2p

high-resolution spectrum (**Figure S4d**) can be assigned to the $2p_{3/2}$ and $2p_{1/2}$ of Ni^{2+} in NiS, respectively, and the two weak humps centered at 860.9 and 876.6 eV are owing to their corresponding satellite peaks.[S4] The peak at 855.5 eV can be assigned to the Ni^{2+} in $Ni(OH)_2$, originating from the hydrolysis of $Ni(OAc)_2$ under hydrothermal conditions.[S1] But $Ni(OH)_2$ was not detected by XRD characterization on the samples, which might be due to the fact that $Ni(OH)_2$ was of poor crystallinity and/or absorbed on the surface of the sample with an amorphous structure, or owing to its low content.

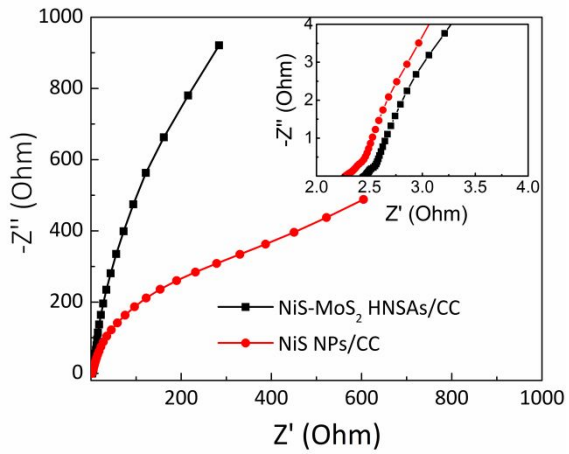

Figure S5 EIS Nyquist plots of the NiS-MoS_2 HNSAs/CC and NiS NPs/CC electrodes, where the inset shows the enlarged view in the range of high frequency.

EIS measurements were further applied to examine the electrochemically kinetic processes. As is seen in **Figure S5**, the NiS-MoS_2 HNSAs/CC electrode shows a larger slope in the low frequency region than NiS NPs/CC, implying a better capacitive behaviour with lower diffusion resistance. And from the enlarged view in the range of high frequency (see the inset in **Figure S5**), both electrodes present a low series resistance (R_s) of about 2.5 Ω, indicating a small internal resistance of the NiS-MoS_2 HNSAs/CC electrode.

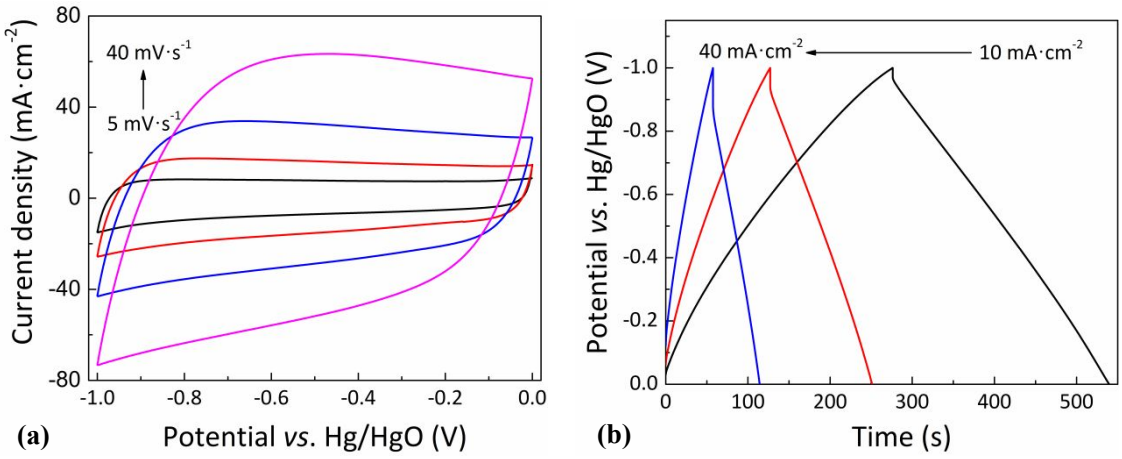

Figure S6. Electrochemical performance of AC/CC electrode. (a) CV curves at different scan rates and (b) GCD curves at different current densities.

The profiles of CV and GCD curves are two macroscopic signs for identifying the energy storage type of an electrode material. As shown in **Figure S6**, the CV and GCD curves exhibits nearly rectangular and triangular shapes, respectively, both of which confirm the ideal double-layer capacitive behavior of the activated carbon/ carbon cloth (AC/CC) negative electrode for a supercapacitor (SC).

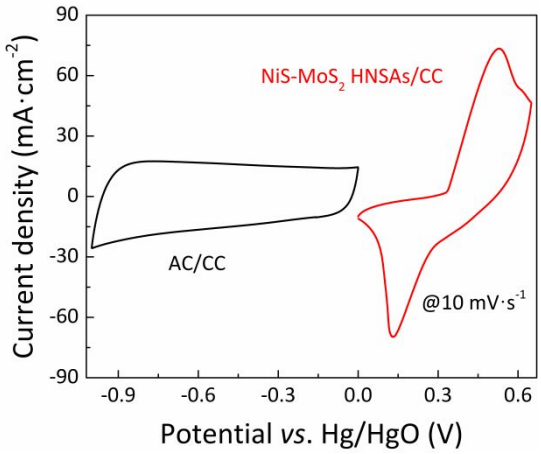

Figure S7. Comparison on CV curves of the AC/CC and NiS-MoS_2 HNSAs/CC electrodes at different potential windows collected at a scan rate of 10 $mV \cdot s^{-1}$.

The comparison on the CV curves of the AC/CC and NiS-MoS_2 HNSAs/CC electrodes at a scan rate of 10 $mV \cdot s^{-1}$ (**Figure S7**) reveals that, the working potential range of the AC/CC electrode was -1.0-0 V, while that of NiS-MoS_2 HNSAs/CC electrode was 0-0.65 V. This result indicates that there is a suitable working potential window between the AC/CC and NiS-MoS_2 HNSAs/CC electrodes. Besides, the capacity of the AC/CC electrode is comparable with that of the NiS-MoS_2 HNSAs/CC electrode. Both results confirm that the present AC/CC and NiS-MoS_2 HNSAs/CC electrodes can be used as a couple of well-matched electrodes for hybrid capacitors.

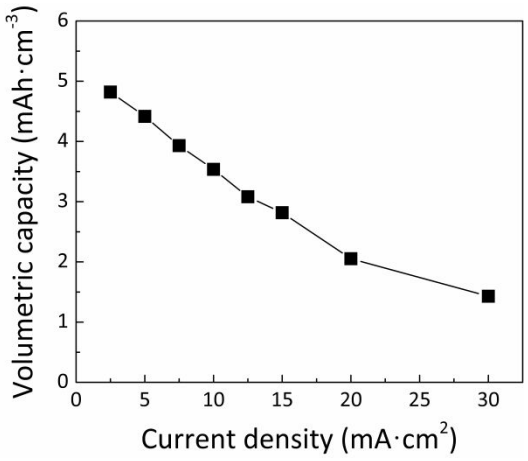

Figure S8. The volumetric capacity versus discharge current density of NiS-MoS_2//AC solid-state hybrid capacitors.

As shown in **Figure S8**, the volumetric capacity of the NiS-MoS_2//AC solid-state hybrid capacitors was calculated from the GCD curves based on the total volume (0.08 cm^3) of the device. The volumetric capacity are 4.82, 4.41, 3.93, 3.54, 3.08, 2.81, 2.05 and 1.43 $mAh \cdot cm^{-3}$ at a current density of 2.5, 5, 10, 12.5, 15, 20 and 30 $mA \cdot cm^{-2}$, respectively.

Table S1. Comparison on the capacity value of NiS-MoS_2 HNSAs/CC electrode with other reported positive electrodes in alkaline aqueous solution

Framework materials*	Electrode materials*	Area capacity (μAh/cm²)	Mass capacity (mAh/g)	Current density	Rate capability	Electrolyte*	Ref.
C cloth	**NiS-MoS_2 HNSAs**	**760**	**271.7**	**2.5 mA/cm²**	**39% (40 mA/cm²)**	**6 M KOH**	**This work**
C cloth	Ni-Mo-S nanosheets	560	312	1 mA/cm²	78.85% (50 mA/cm²)	KOH	2
C cloth	$Ni_{0.54}Co_{0.46}O_2$ nanosheet arrays	438	238.1	1 mA/cm²	90.3% (50 mA/cm²)	2 M KOH	44
C cloth	H-TiO_2@$Ni(OH)_2$ nanowire arrays	612	306	1 mV/s	65% (100 mV/s)	6 M KOH	45
C nanotube fiber	$CoNiO_2$@$Ni(OH)_2$ nanowire arrays	674.1	539.3	1 mA/cm²	69.8% (10 mA/cm²)	3 M KOH	46
C nanofibers	$Ni(OH)_2$ nanoplate	-	208.4	5 mV/s	92% (40 mV/s)	6 M KOH	47
C cloth	NiCoP@NiCoP nanowire arrays	-	312	1 A/g	78% (10 A/g)	3 M KOH	S5
Graphite fibers	Ni-Co-N/$NiCo_2O_4$ nanosheets	-	384.75	4 A/g	86.5% (20 A/g)	3 M KOH	S6
Ni foam	Co-Cd-Se nanorods	384	192	1 A/g	76% (15 A/g)	2 M KOH	S7
Ni foam	Zn-Co-S nanowires	900	366.7	3 mA/cm²	62% (40 mA/cm²)	6 M KOH	S8
Ni foam	NiSe@$MoSe_2$ nanosheet arrays	-	128.2	1 A/g	76% (15 A/g)	2 M KOH	S9
Ni foam	Ni_3Se_2@$Ni(OH)_2$ nanocomposite	1689	281.5	3 mA/cm²	66.8% (40 mA/cm²)	3 M KOH	S10
Cu fibers	NiO NSs@CNTs @CuO nanowire arrays	-	230.48	2 A/g	76.83% (25 A/g)	1 M KOH	S11
Co foam	VS_4/rGO/CoS_2@Co nanocomposite	-	274.3	0.625 A/g	35% (6.25 A/g)	1 M KOH	S12

* C: Carbon
M: mol·L^{-1}

REFERENCES

(S1) Guan, S. D.; Fu, X. L.; Zhang, Y.; Peng, Z. J. beta-NiS modified CdS nanowires for photocatalytic H_2 evolution with exceptionally high efficiency. *Chem. Sci.* **2018,** *9* (6), 1574-1585, DOI: 10.1039/c7sc03928j.

(S2) Liu, N.; Guo, Y. L.; Yang, X. Y.; Lin, H. L.; Yang, L. C.; Shi, Z. P.; Zhong, Z. W.; Wang, S. N.; Tang, Y.; Gao, Q. S. Microwave-assisted reactant-protecting strategy toward efficient MoS_2 electrocatalysts in hydrogen evolution reaction. *ACS Appl. Mater. Interfaces* **2015,** *7* (42), 23741-23749, DOI: 10.1021/acsami.5b08103.

(S3) Yu, X. Y.; Feng, Y.; Jeon, Y.; Guan, B.; Lou, X. W.; Paik, U. Formation of Ni-Co-MoS_2 nanoboxes with enhanced electrocatalytic activity for hydrogen evolution. *Adv. Mater.* **2016,** *28* (40), 9006-9011, DOI: 10.1002/adma.201601188.

(S4) Nesbitt, H. W.; Legrand, D.; Bancroft, G. M. Interpretation of Ni2p XPS spectra of Ni conductors and Ni insulators. *Phys. Chem. Miner.* **2000,** *27* (5), 357-366, DOI: DOI 10.1007/s002690050265.

(S5) Zhu, Y. L.; Zong, Q.; Zhang, Q. L.; Yang, H.; Wang, Q. Q.; Wang, H. Y. Three-dimensional core-shell NiCoP@NiCoP array on carbon cloth for high performance flexible asymmetric supercapacitor. *Electrochim. Acta* **2019,** *299*, 441-450, DOI: 10.1016/j.electacta.2019.01.043.

(S6) Tan, H.; Liu, Z. H.; Chao, D. L.; Hao, P.; Jia, D. D.; Sang, Y. H.; Liu, H.; Fan, H. J. Partial nitridation-induced electrochemistry enhancement of ternary oxide nanosheets for fiber energy storage device. *Adv. Energy Mater.* **2018,** *8* (21), 1800685, DOI: 10.1002/aenm.201800685.

(S7) Zhai, Z. B.; Huang, K. J.; Wu, X. Superior mixed Co-Cd selenide nanorods for high performance alkaline battery-supercapacitor hybrid energy storage. *Nano Energy* **2018,** *47*, 89-95, DOI: 10.1016/j.nanoen.2018.02.059.

(S8) Li, C.; Balamurugan, J.; Kim, N. H.; Lee, J. H. Hierarchical Zn-Co-S nanowires as advanced electrodes for all solid state asymmetric supercapacitors. *Adv. Energy Mater.* **2018,** *8* (8), 1702014, DOI: 10.1002/aenm.201702014.

(S9) Peng, H.; Zhou, J. Z.; Sun, K. J.; Ma, G. F.; Zhang, Z. G.; Feng, E.; Lei, Z. Q. High-performance asymmetric supercapacitor designed with a novel NiSe@$MoSe_2$ nanosheet array and nitrogen-doped carbon nanosheet. *ACS Sustainable Chem. Eng.* **2017,** *5* (7), 5951-5963, DOI: 10.1021/acssuschemeng.7b00729.

(S10) Shi, X.; Key, J.; Ji, S.; Linkov, V.; Liu, F.; Wang, H.; Gai, H.; Wang, R. $Ni(OH)_2$ nanoflakes supported on 3D Ni_3Se_2 nanowire array as highly efficient electrodes for asymmetric supercapacitor and Ni/MH battery. *Small* **2018**, e1802861, DOI: 10.1002/smll.201802861.

(S11) Nagaraju, G.; Sekhar, S. C.; Yu, J. S. Utilizing waste cable wires for high-performance fiber-based hybrid supercapacitors: an effective approach to electronic-waste management. *Adv. Energy Mater.* **2018,** *8* (7), 1702201, DOI: 10.1002/aenm.201702201.

(S12) Wang, S. Q.; Song, Y. P.; Ma, Y.; Zhu, Z. Q.; Zhao, C. H.; Zhao, C. J. Attaining a high energy density of 106 Wh kg^{-1} for aqueous supercapacitor based on VS4/rGO/Cos_2@Co electrode. *Chem. Eng. J.* **2019,** *365*, 88-98, DOI: 10.1016/j.cej.2019.02.031.